High-space resolution imaging plate analysis of extreme ultraviolet (EUV) light from tin laser-produced plasmas

Review of Scientific Instruments

High-space resolution imaging plate analysis of extreme ultraviolet (EUV) light from tin laser-produced plasmas

Cite as: Rev. Sci. Instrum. **88**, 033506 (2017); https://doi.org/10.1063/1.4978526
Submitted: 25 October 2016 • Accepted: 27 February 2017 • Published Online: 21 March 2017

Christopher S. A. Musgrave, Takehiro Murakami, Teruyuki Ugomori, et al.

High-space resolution imaging plate analysis of extreme ultraviolet (EUV) light from tin laser-produced plasmas

Christopher S. A. Musgrave,[1] Takehiro Murakami,[1] Teruyuki Ugomori,[2] Kensuke Yoshida,[2] Shinsuke Fujioka,[2] Hiroaki Nishimura,[2] Hironori Atarashi,[1,a)] Tomokazu Iyoda,[1] and Keiji Nagai[1,b)]

[1]*Iyoda Supra-Integrated Material Project, Exploratory Research for Advanced Technology (ERATO), Japan Science and Technology Agency, and Frontier Research Center, Tokyo Institute of Technology, 4259-S2-3 Nagatsuta, Midori-ku, Yokohama 226-8503, Japan*

[2]*Institute of Laser Engineering, Osaka University, 2-6 Yamada-Oka, Suita, Osaka 565-0871, Japan*

(Received 25 October 2016; accepted 27 February 2017; published online 21 March 2017)

With the advent of high volume manufacturing capabilities by extreme ultraviolet lithography, constant improvements in light source design and cost-efficiency are required. Currently, light intensity and conversion efficiency (CE) measurments are obtained by charged couple devices, faraday cups etc, but also phoshpor imaging plates (IPs) (BaFBr:Eu). IPs are sensitive to light and high-energy species, which is ideal for studying extreme ultraviolet (EUV) light from laser produced plasmas (LPPs). In this work, we used IPs to observe a large angular distribution (10°-90°). We ablated a tin target by high-energy lasers (1064 nm Nd:YAG, 10^{10} and 10^{11} W/cm^2) to generate the EUV light. The europium ions in the IP were trapped in a higher energy state from exposure to EUV light and high-energy species. The light intensity was angular dependent; therefore excitation of the IP depends on the angle, and so highly informative about the LPP. We obtained high-space resolution (345 μm, 0.2°) angular distribution and grazing spectrometer (5-20 nm grate) data simultaneously at different target to IP distances (103 mm and 200 mm). Two laser systems and IP types (BAS-TR and BAS-SR) were also compared. The cosine fitting values from the IP data were used to calculate the CE to be 1.6% (SD ± 0.2) at 13.5 nm 2% bandwidth. Finally, a practical assessment of IPs and a damage issue are disclosed. [http://dx.doi.org/10.1063/1.4978526]

I. INTRODUCTION

Extreme ultraviolet lithography (EUVL) is considered to be the most promising technology for the production of the next-generation of integrated circuits.[1–3] The current light source, argon fluoride (ArF) lasers, complies with Moore's law[4] by utilizing many techniques such as water immersion and multi-patterning.[5] However, the limits of these techniques are now being reached. EUVL aims to provide a light source of requisite resolution that does not require additional processing techniques. To produce the lithographic light, the extreme ultraviolet (EUV) light source utilizes EUV light from laser-produced plasmas (LPPs), which produces highly efficient 13.5 nm EUV.[6] Recently, power of 100 W at the intermediate focus has been obtained through improvements to the entire EUVL system by the use of liquid tin droplets.[7,8] Yet, for EUVL high volume manufacturing (HVM) to be viable, the power at the intermediate focus must be greater than 240 W. Therefore any improvements that could increase the power and cost-efficiency of the system would be welcome.[9] Furthermore, these improvements are important as EUV lithography technology is now scaling into compact sizes by use of gas puff targets and lower powered lasers.[10,11]

Imaging plates (IPs) is a technique that has been successfully used to study x-rays in very high-energy plasma physics experiments.[12–14] An IP consists of a photostimulable material mounted on a flexible polymer film that contains europium ions that can be excited when exposed to photons and high-energy species. When exposed, the europium ions (Eu^{2+} to Eu^{3+}) in the film are trapped in higher energy state lattice defects called F centers. A reading apparatus scans the IPs, which returns the europium ions to the ground state and releases a photon. The digitized image captures space and intensity resolution. Furthermore, IPs have been used to capture hot electron angular distribution information before.[13]

To date, little data exists on the angular distribution of EUV despite sensitivity to 13.5 nm light.[15] Obtaining angular distribution data can often be a issue of practicality in regular vacuum chambers. In these experiments, EUV angular distribution was measured at a small selection of singular points, for example, three points at 45°, 60°, and 90°.[16,17] Other work has used a calorimeter in incremental steps to achieve a full angular distribution.[18] Although valuable, these are low-space resolution measurements that could be losing data because the entire distribution was not measured or the increments were large. High-space resolution data could influence aspects of

a)Present address: Graduate school of Environmental and Life Science, Okayama University, 3-1-1 Tsushima-naka, Kita-ku, Okayama 700-8530, Japan.
b)Author to whom correspondence should be addressed. Electronic mail: nagai.k.ae@m.titech.ac.jp

EUVL light sources such as mirror design, target size, or laser pulse widths. To obtain high-space resolution measurements using these techniques, the cost would be too substantial or require an impractical amount of time. However, phosphor imaging plates are a relatively low cost and practical alternative to obtain high-space resolution EUV angular distribution data. Furthermore, IPs can be used in many existing vacuum chambers regardless of size. The flexible imaging plates can be placed inside the vacuum chamber at an angular distribution of the users choice. The photosensitive films will emit photostimulated luminescence (PSL) on exposure to EUV light and other high-energy species. Protective films or filters can be used to shield the plate from unwanted species to select the species that interacts with the phosphor film. An imaging plate reader can scan the entire imaging plate to obtain an intensity distribution without the need to perform additional experiments at different angles.

In addition, the practicality of the imaging plate must be considered as it is exposed to many high-energy species that could affect the resulting data. Imaging plate errors and damage have been well-documented by the medical profession.[19] Data acquisition errors and physical damage can occur from incorrect exposure settings, through the mechanical scanning process, and dust contamination. This information is useful to our investigation into the use of imaging plates for the study of EUV from LPPs.

This aim of this work was to analyze EUV light from tin LPPs across a large angular distribution of 10°-90° with high-space resolution. We also assess the practicality of using IPs from the damage sustained during the experimental process. Moreover, we used the high-space resolution data to obtain a cosine distribution of the EUV light and calculate the conversion efficiency (CE). Two different Nd:YAG laser sources and imaging plate types were used to ensure a thorough analysis for the validity of IPs. The EUV laser facility at the Institute of Laser Engineering, Osaka is a national users facility in Japan. This was to ensure that the laser-produced EUV light was credible. In addition, the laser pulse width could be selected, which was not available to the Tokyo Institute of Technology. At the Tokyo Institute of Technology, our interest was to use laser conditions more accessible to researchers in this field. Imaging plates were determined to be a fast and informative technique to analyze EUV light from tin LPPs. This technique could be applied in the design of future EUV light sources.

II. EXPERIMENTAL DETAILS AND SET-UP

In all experiments, a high purity, planar tin target (100 μm thick, Nilaco, Japan) was the source for EUV generation. The laser used at the Tokyo Institute of Technology (Tokyo Tech) was a 1064 nm diode pumped Nd:YAG laser (L11038-01 Hamamatsu Photonics, Japan) with a 1 ns pulse width and a pulse energy of 2 mJ. The laser spot size was measured to be 55 μm from polystyrene film ablation[20] producing an intensity of 1.6×10^{11} W/cm^2. A grazing incidence spectrometer (GIS) with a 5-20 nm grating fitted with a CCD (Tokyo Instruments, TIUV 235-920) was used to record the EUV spectra. The focusing lens was placed inside the chamber and had an F value of 200, with the lens to target distance of 219 mm. A schematic diagram for the experimental setup is given in Fig. 1.

Imaging plate experiments were performed in the Institute of Laser Engineering (ILE), Osaka with the EUV-DB laser,[21] a 1064 nm Nd:YAG laser with a spot size of 200 μm. Two different pulse widths were used: 7.9 ns and 3.6 ns with the corresponding pulse energies of 610 mJ and 230 mJ, respectively. The laser intensity was therefore 5.9 $\times 10^{10}$ and 5.4×10^{10} W/cm^2, respectively. A grazing incidence spectrometer (GIS) with a 5-20 nm grating was used to record the EUV spectrum. These light intensities were chosen based on the previous optimization for 13.5 nm generation.[22,23]

The target vacuum chamber pressure was typically in the order of 1×10^{-5} Torr. The phosphor imaging plates (Fujifilm, Japan) consisted of a BaFBr:Eu^{2+} photosensitive film, and the BAS-TR type was used exclusively at Tokyo Tech. Imaging plate experiments performed at ILE, Osaka used the BAS-SR phosphor imaging plate type (Fujifilm, Japan), which has a protective mylar layer covering the photosensitive film. The dimensions of the imaging plates varied depending on the distance between the target and imaging plate; at 103 mm target to imaging plate distance, typically 36 mm × 126 mm plates were used, and at 200 mm distance 50 mm × 250 mm were used. A Rigaku RAXIA-Di imaging plate reader was used to scan the imaging plates after EUV illumination to convert the data into an intensity versus observed angular distribution image. The scanning resolution was set to 50 μm (equivalent to 0.03° for 103 mm and 0.01° for 200 mm distances).

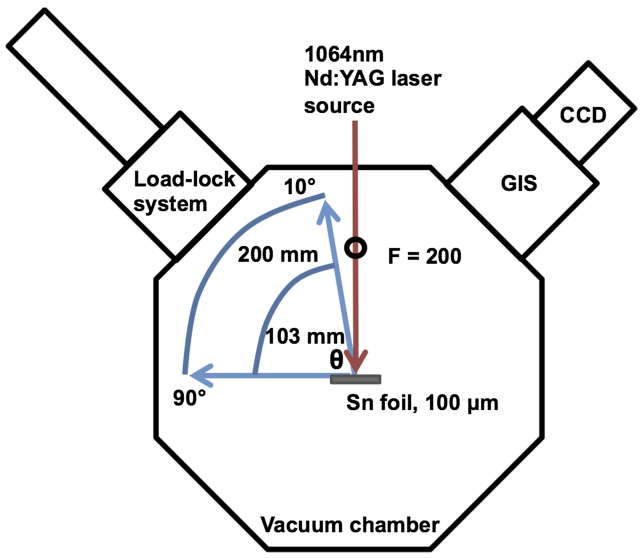

FIG. 1. A schematic diagram of the experimental setup used at Tokyo Tech to obtain EUV and imaging plate data. A load-lock system was used to insert targets/imaging plates into the chamber under vacuum conditions. This allowed for quick insertion and removal of the IPs. The distance from the target to the imaging plate was equidistant at all observed angles. The outer, larger line in the schematic represents 200 mm target to IP distance, whereas the inner, smaller line represents 103 mm target to IP distance. The GIS and entrance aperture were 45° with respect to the target. The setup at ILE, Osaka, of the vacuum chamber used the same specifications as the Tokyo Tech experiments.

Some experiments at Tokyo Tech used a zirconium filter (NTT-AT, Japan) to eliminate other radiation/high-energy species so that only EUV light exposed the IPs. The Zr film dimensions were 10 mm × 80 mm and 100 nm thick. Including the Zr film and frame, the total dimensions were 20 mm × 90 mm × 8 mm. The Zr film was free standing (no polymer support) and had no additional coating. The filter transmission for 13.5 nm light was about 35% from the EUV spectrum and IP data obtained at Tokyo Tech. This is in agreement with previous data.[24] The filter was placed between the target and imaging to ensure that the laser was not blocked but gave the largest angular distribution possible. The angles observed were 10° to 80° or 20° to 90° at 103 mm target to IP distance, however the angle was reduced slightly due to the bulky frame. At 200 mm target to IP distance, the angles observed were 10°-72° or 18°-90°. The placing of the filter was determined by referencing from the target to IP positions to ensure an accurate placement by the load-lock delivery system. Additionally, the load-lock system at Toyko Tech could allow quick removal of the IPs. They could be scanned within 10 min of exposure, which is below the fade-time for IPs.[25]

The imaging plate data were fitted to a cosine function that is described elsewhere.[16] The IP data obtained at Tokyo Tech were fit from 20° to 90° (or the maximum distribution observed). The IP data obtained at ILE, Osaka were fit from 35° to 85°.

III. RESULTS

A. EUV spectra and imaging plate data

Typically, the raw data for each experimental condition tested can be seen in Figs. 2 and 3. All the imaging plate data obtained are summarized in Table I. The Zr filter frame blocked incoming light and high-energy species creating the thick black edge seen in Figs. 3 and 8. In each experiment, a typical EUV spectrum from tin plasma was obtained with a strong peak around 13.5 nm. The emission has been characterized as an unresolved transmission array (UTA) from Sn^{8+} to Sn^{21+} as 4d-4f transmission[26] typically obtained from laser intensities of 10^{10} W/cm^2 from Nd:YAG lasers.[27] The

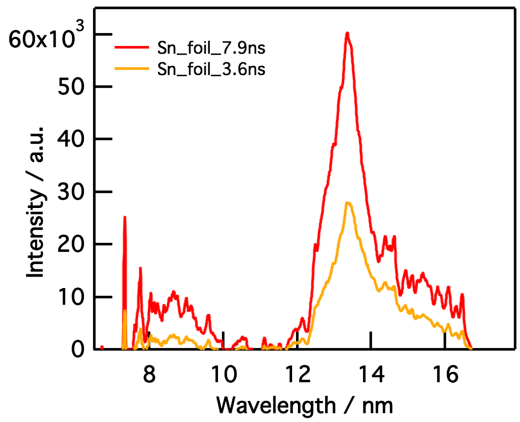

FIG. 2. The EUV spectra for the experiments performed at ILE, Osaka. The shorter wavelengths appeared due to the increased electron temperature caused by the longer pulse durations.[27] This was not observed at Tokyo Tech due to the shorter pulse duration used.

condition of the target affected the observed EUV and IP intensity. Ablated oxygen atoms from an oxidized Sn surface reabsorbed more of the generated EUV than that compared to a clean tin surface resulting in a lower intensity. Furthermore, the IP intensities were affected by factors such as time from exposure to IP reading (Table II). For experiments where the IP holder was removed quickly from the chamber, the corresponding light intensity was high. Conversely, if a long time was required, a lower light intensity was measured. The intensity of the Zr filtered IP data was 30% of the non-filtered data at 103 mm, which was in accordance with the transmission of Zr filters for 13.5 nm light.[24] In addition, the intensity at 200 mm was 35% of the 103 mm non-filtered IP data. This was proportional to the solid angle for these distances.

The IP sensitivity to EUV photons around 13.5 nm was estimated to be 1.6×10^{-4} PSL/photon at 1.8×10^{-6} J/cm^2 estimated by a calorimeter. The total PSL was calculated from the integration of the IP data. The calorimeter was used to estimate the number of EUV photons. This value was slightly lower compared to previous literature for BAS-TR IP sensitivity in the 20-40 eV range.[28] However, there was likely

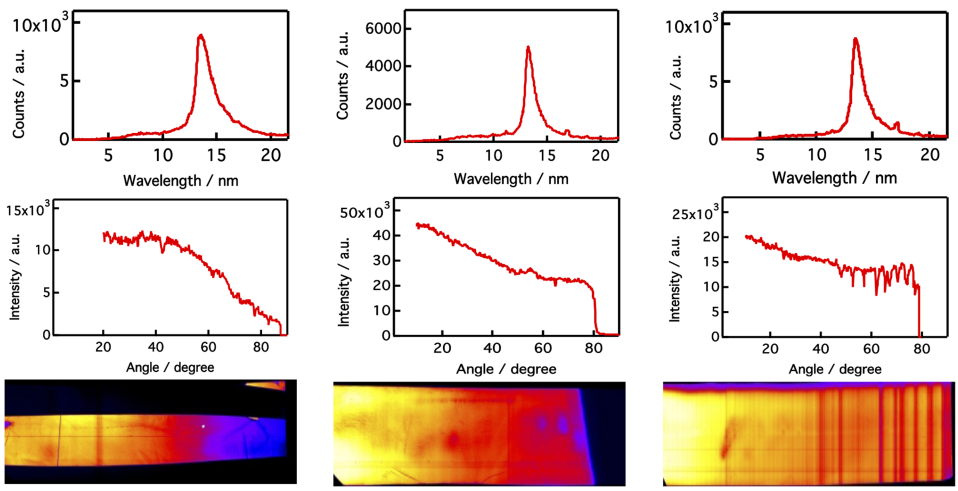

FIG. 3. The typical EUV spectra, imaging plate data, and images for each of the experimental conditions tested at Tokyo Tech. The columns are for the different target to IP distances of 103 mm with Zr filter (left), 103 mm without Zr filter (middle), and 200 mm without Zr filter (right). The intensity of the EUV spectrum was affected by oxidation of the tin target. This was unavoidable in experiments at 200 mm target to IP distance requiring the entire vacuum chamber to be returned to atmospheric pressure in order for the IP to be removed. The 103 mm with Zr filter and 200 mm data images show examples of slight mechanical roller errors. In both cases, the resulting data were not affected.

TABLE I. Summary of the imaging plate data obtained from all laser experiments.

IP type	Distance target to IP (mm)	Laser pulse width (ns)	Average $\cos^X \theta$ fitting value	Notes
BAS-SR	200	7.9	0.6	
	200	3.6	0.6	
BAS-TR	103	1.0	0.4	Zr filtered
	103	1.0	3.7	
	200	1.0	3.0	

TABLE II. Absolute intensity of the IP data for experiments performed at Tokyo Tech.

	Absolute value for peak intensity (arb. units)		
Shot number	103 mm Zr filter	103 (mm)	200 (mm)
1	25×10^3	45×10^3	15×10^3
2	12×10^3	50×10^3	14×10^3
3	10×10^3	25×10^3	20×10^3
4	3×10^3	45×10^3	12×10^3
5	12×10^3	45×10^3	14×10^3
6		45×10^3	
Average	12.4×10^3	42.5×10^3	15×10^3

a small error due to the lack of accurate calibration and from signal fading of the IPs.

B. Imaging plate fitting diagrams

The imaging plate fitting curves for all experiments are given in Figs. 4–7. Fig. 4 shows the results from the experiments performed at ILE, Osaka. Figs. 5–7 shows the results from the experiments performed at Tokyo Tech. All data were obtained by a single laser shot and were normalized to 1 at 20° from data collected at Tokyo Tech, and 35° from data collected at ILE, Osaka. Each line in each figure represents the IP exposed to an individual laser shot.

The $\cos^X \theta$ fitting values for X for BAS-TR imaging plates exposed without a Zr filter were affected by the other high-energy species (ions, neutral particles) produced on ablation rather than the shorter EUV wavelengths. Furthermore, in experiments that used BAS-TR imaging plates without a Zr filter, the target cleanliness and/or deformations would also have affected the $\cos^X \theta$ fitting values for X, where X = 3.7 and 3.0.

The $\cos^X \theta$ fitting values for X, where X = 0.4, obtained from experiments performed at ILE, Osaka were close to the case with Zr filter from BAS-TR imaging plates, rather than that without Zr filter measured at Tokyo Tech.

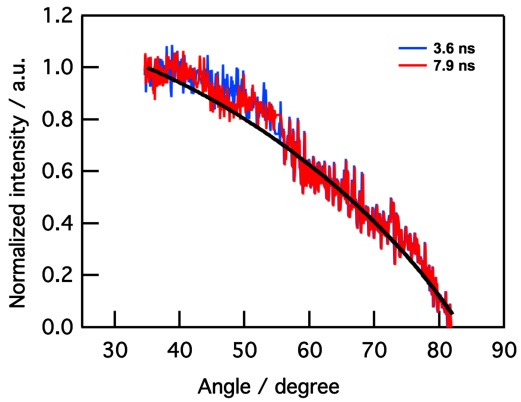

FIG. 4. Imaging plate data obtained at ILE, Osaka. The target to IP distance was 200 mm. $\text{Cos}^X \theta$ (black) fitting value, where X = 0.6, was obtained for both 7.9 ns (red) and 3.6 ns (blue) pulse durations. Only one fitting curve can be seen because both curves overlap each other.

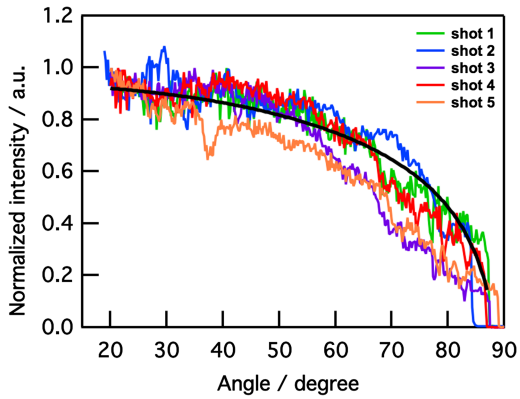

FIG. 5. Imaging plate data, with Zr filter, obtained at Tokyo Tech. The target to IP distance was 103 mm. The average $\cos^X \theta$ fitting value (black), where X = 0.4, was obtained. The Zr filter reduced the effect of incoming ions, electrons, and debris, increasing the consistency of the data compared to the data in Fig. 6.

C. Imaging plate damage from high-energy species

Fig. 8(a) compared to Fig. 8(b) demonstrated that the damage to the BAS-TR IPs was mainly localized to the plane of the laser (defined by the plane of the laser and the GIS position). For an unprotected BAS-TR IP, the damage to the film was noticeable only after 5 shots. By comparison, little or no damage was observed after 15 shots when using a Zr filter (Figs. 8(c) and 8(d)). We also considered that the damage could

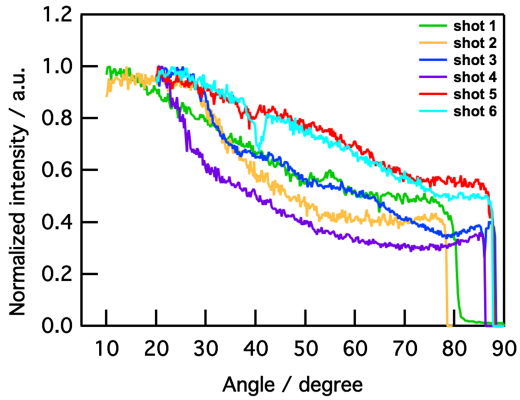

FIG. 6. Imaging plate data, without Zr filter, obtained at Tokyo Tech. The target to IP distance was 103 mm. The average $\cos^X \theta$ fitting value, where X = 3.7 (fitting lines are not shown), was obtained. The IP at this distance was exposed to the effects of ions, electrons, and debris from the ablated target. In addition, factors such as the oxidized tin layer, dust, or deformations in the target surface affected the cosine fitting values significantly. The result was that the fitting values were more inconsistent.

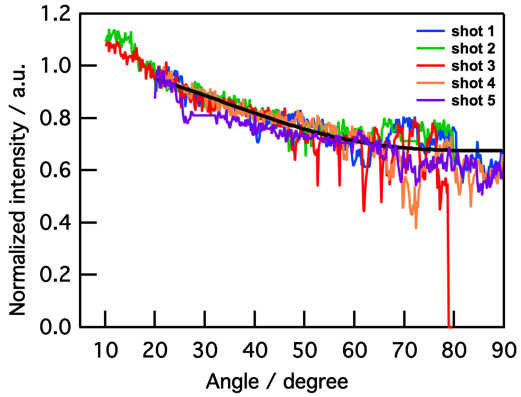

FIG. 7. Imaging plate data, without Zr filter, obtained at Tokyo Tech. The target to IP distance was 200 mm. The average $\cos^X \theta$ fitting value (black line), where X = 3.0, was obtained. The data were smoothed in some regions where the scanning errors were noticeable.

have occurred from the IP reader. If the IP reader caused damage to the IP, the IP images would show evidence irrespective of the presence of a Zr filter. BAS-TR plates do not have a mylar film protection, however, only the non-Zr filtered IP images showed degradation. Thus we determined that the source of the damage was from high-energy species and not from the imaging plate reader. The top right corner of the Zr filtered experiments in Figs. 8(c) and 8(d) showed examples where the Zr filter did not block the incoming radiation. This did not affect the resulting data. The uncovered areas clearly demonstrated the difference in IP exposure between the filtered and non-filtered areas.

IV. DISCUSSION

A. EUV and imaging plate data

At ILE, Osaka (Figs. 2 and 4), there were two parameters tested: (1) The laser pulse duration was chosen to be either 8 ns or 3 ns, and (2) use of a BAS-SR imaging plate. The laser pulse length determined the laser intensity, and affected the size and shape of the resulting plasma.[29,30] The BAS-SR IP was chosen because of the protective mylar film on the surface of the plate. The mylar film performed as a filter for other radiation species produced on ablation of the tin target. These factors were reflected in the $\cos^X \theta$ fitting values for X, where X = 0.6 for both laser pulse durations. The filtering effect was clear when compared to the BAS-TR IP $\cos^X \theta$ fitting value for X, where X = 3.0, at the same distance (Fig. 7). A $\cos^{0.6} \theta$ fitting value is in agreement to the previous EUV calorimeter data under similar conditions.[16] This meant that these pulse durations did not have a significant impact to the ablated species to affect the angular distribution. The longer pulse durations increased the heating of tin, into the region of 100 eV, producing the shorter EUV wavelengths (<10 nm) observed in Fig. 2. The integration of these shorter wavelengths revealed that they were actually a small component of the entire spectrum, therefore did not expose the IP and so did not affect the $\cos^X \theta$ fitting values. In addition, the mylar film on the BAS-SR imaging plate would have absorbed such small contributions from these shorter wavelengths. The shorter pulse duration (1.0 ns) at Tokyo Tech did not heat the tin target sufficiently to produce the shorter EUV wavelengths below 10 nm. The majority of the EUV emission was in the 10-15 nm region, corresponding to 20-40 eV. The imaging plate type and target to IP distance were more important in determining the $\cos^X \theta$ fitting values. The mylar layer operated as a filter to incoming radiation and so sensitivity was lost that could likely distinguish between the two pulse durations such as out-of-band radiation or absorption of EUV.

At Tokyo Tech, the two main parameters of interest were (1) selecting the target to IP distances of either 103 mm or 200 mm, and (2) use of a BAS-TR imaging plate with or without a Zr filter. $\mathrm{Cos}^X \theta$ fitting values for X, where X = 3.7 and X = 3.0, were obtained by BAS-TR IPs without a Zr filter at distances of 103 mm and 200 mm, respectively (Figs. 6 and 7). These values indicated that they were exposed to more than just EUV light, which was expected given the BAS-TR IPs did not have a protective film or Zr filter to absorb incoming radiation. An increased $\cos^X \theta$ fitting value for X, where X > 0.6, would normally indicate that an optically thick opaque plasma surrounding a 13.5 nm emissive plasma was produced.[15] The EUV spectrum we obtained when acquiring BAS-TR IP data does not show this strong reabsorption in the 13.5 nm region. Strong EUV reabsorption is observed when lasers in higher harmonics are used.[26] This meant that the higher coefficients were a direct result of the other radiation species rather than from an optically thick opaque plasma surrounding a 13.5 nm emissive plasma. Another interesting feature was that the $\cos^X \theta$ fitting values for X were similar at both 103 mm and 200 mm distances, where X = 3.7 and X = 3.0, respectively. However, at 200 mm the consistency of the IP exposure was much greater than that at 103 mm. The unprotected IPs were exposed by light, high-energy species, and neutral debris, which increased the $\cos^X \theta$ fitting values compared to the Zr filtered experiments. The IPs exposed at 200 mm light intensity was only 1/4 than that at 103 mm, in accordance with the solid angle for

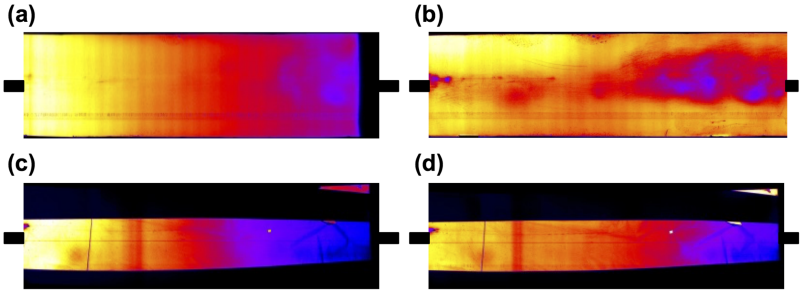

FIG. 8. Images of a new imaging plate after the first exposure (a) and the same imaging plate after the sixth exposure (b) to EUV light and other high-energy species. The IP shows the effect of high-energy species such as ions damaging the phosphor film. Images (c) and (d) were obtained by exposing an imaging plate with a Zr filter placed between the target and the IP. The Zr filtered images show that very little damage was sustained after 15 exposures. The black marks denote the plane of the laser.

these distances. This was reflected by the reduction in $\cos^X \theta$ fitting values for X, from X = 3.7 to X = 3.0. This can be justified by the loss of energy from the neutral debris and high-energy species exposing the IPs. The drop-off in energy meant that only the highest energy species could expose the IP, increasing the fitting consistency.

The BAS-TR experiments with a Zr filter (Fig. 5) obtained $\cos^X \theta$ fitting values for X, where X = 0.4. This was very similar to those obtained using the BAS-SR IPs in the ILE, Osaka experiments, and to previous literature reports using EUV calorimeter data.[16] This confirmed that the other high-energy species present on ablation increased the value of X in the $\cos^X \theta$ fitting equation in the non-filtered experiments using BAS-TR IPs (Figs. 6 and 7). Our Zr filter had 35% transmission, which was in agreement with the 30% transmission measured by the Zr filtered IP compared to the unfiltered IP at the same distance. In this case, the ratio of filtered to non-filtered IP intensity was 1:3.2. This ratio is much larger than the ratio of 1:1.8 obtained by other researchers.[31] However, in their work only the ratio of light radiation was measured. Our ratio can be accounted for by the fact that the non-filtered IPs were exposed to significantly more higher energy species than the Zr filtered IPs. Regarding the EUV light systems, both BAS-TR and BAS-SR IPs are relevant; for example, a BAS-TR IP could be used to study the species produced by different plasma types. This could then be used to estimate the effect on the collection mirror rather than the damage of expensive optics from ions or debris. Our data indicated that BAS-SR plates would suffice if EUV was the only parameter of interest.

A critical aspect of the imaging plate technique was the high space resolution data it provided. From the raw data set, the space resolution was calculated to be 345 μm, equivalent to 0.2° on the IP. The scanning resolution limit of the reader was 50 μm but lower resolution (>50 μm) is often obtained due to factors such as the quality of the imaging plate or the imaging plate reader. Other researchers have shown that the limits of space resolution for BAS-TR IPs to be below 100 μm.[12,32] Therefore, our results are well within reason and still represent a significant gain in data accuracy when considering angular distribution of EUV from Sn LPPs. Increased accuracy of angular distribution data presented here raises accuracy questions about angular distribution data from other techniques reported from so few data points. The issue with singular point measurements across a large distribution is that the accuracy of derived information such as conversion efficiency can be lost or inaccurate.

It was pertinent to use the IP data to obtain the conversion efficiency (CE) from the laser energy to EUV at 2% bandwidth for the laser used at Tokyo Tech. The laser CE at 2% bandwidth was calculated to be 1.6% (0.2 SD) using the following:

$$CE = \int_0^{2\pi} \int_0^{\pi/2} \left[E_{cal(45)}/I(45)\right] I(\theta) d\theta d\Omega, \qquad (1.1)$$

where $E_{cal(45)}$ is the ratio of the energy at 13.5 nm 2% bandwidth from the measured energy from an energy calorimeter at 45°, and Equation (1.1) is described in more detail elsewhere.[17] The ratio of out-of-band energy to the in-band energy allowed calculation of the in-band energy, where the ratio of in-band to out-of-band is 1:1.8.[30] Thus the ratio of the energy at 13.5 nm 2% bandwidth in-band was obtained. With the $\cos^X \theta$ value for X = 0.4, for the IP data that used a Zr filter, and knowing the in-band energy, the CE at 2% bandwidth was calculated. 1.6% was consistent with previous reports for the ablation of planar Sn targets using a Nd:YAG laser.[21,30,33] While 1.6% was not highly efficient, however the purpose of our experiments was not to optimize the laser system but demonstrate the usefulness of IPs. The data from the filtered IP represent only the EUV light exciting the IP rather than non-filtered experiments that produced larger $\cos^X \theta$ fitting values for X. In the context of EUV sources, IPs can be used to improve measurements of derived information, which in turn could aid in the optimization or design of EUV light sources. For example, if the target type or the laser pulse sequence is changed, IPs can be used to form a more accurate comparison between these parameters. Furthermore, IPs could easily be implemented in other LPP studies. For example, beyond EUV (sub 13.5 nm) candidates currently suffer from much lower efficiencies compared to Sn EUV light sources.[34,35]

B. Imaging plate damage and a practical assessment of imaging plates

During the data collection stage of this work, some IP damage/data errors were encountered. Fig. 8 demonstrates degradation of the phosphor film over time, with small dark spots growing after each use of the imaging plate. Damage from high-energy species was only apparent with the BAS-TR imaging plate type, and not the BAS-SR type. The lifetime of the IPs was very low without a protective mylar layer or a Zr filter. However, BAS-TR IPs protected by a Zr filter showed very little damage after 15 or more shots. This confirmed that ions and/or neutral particles, not photons, were the main sources of damage to the phosphor film. The reason for using the BAS-TR imaging plate was to determine what species the imaging plate would observe in order to better study tin LPPs. In some experiments, a BAS-TR imaging plate could be informative, but may not be suitable in a system where the repetition rate will dramatically increase the IP exposure to ions and debris. The BAS-SR imaging plate was sufficient for an EUV analysis and the protective layer ensured a long plate lifetime. Exposing the BAS-SR plate to multiple successive shots would be valuable at determining the effectiveness of the mylar layer in conditions closer to an EUV system.

Scanning errors due to the reader mechanical roller errors happened occasionally. The IP reader uses mechanical rollers to physically push the imaging plate through the reader. In situations where this mechanism does not operate correctly, or slips, errors appear as absolute dark areas in the final image. These areas were devoid of any light intensity. Smaller scanning errors occurred too, which manifested as a darker color to the surrounding area (Fig. 8(d)), i.e., a vertical red bar/line surrounded by an area of yellow/orange, etc. Experiments at 103 mm target to IP distance rarely suffered from this error due to the smaller plate size. On the other hand, at 200 mm

target to IP distance, small scanning errors occurred more frequently. The most likely explanation was that these IPs were much larger (250 mm vs 127 mm) and so had to pass through the mechanical rollers for longer giving more chance for an error to occur. Another consideration was that these errors could have occurred due to the apparatus we used, assuming newer machines only suffer from scanning errors very infrequently.

For the practical use to monitor LPP-EUV, imaging plates can suffer from damage/data errors from the high-energy species produced on target ablation or from the imaging plate reader. To increase the IP lifetime, an IP with a protective layer or a Zr filter is highly desirable. Despite the risks, imaging plates are very effective at observing EUV light and very easy to use. The flexible plates can be used to observe a large angular distribution offering a distinct advantage over other methods. To analyze EUVL systems, sufficient protection for the IP is highly recommended.

V. CONCLUSION

With the advent of high volume manufacturing by EUVL, constant improvements to light sources are essential. The motivation for this work was to develop a high-space resolution technique that could be implemented into the design of EUV light sources to improve system efficiency. This work demonstrated that phosphor imaging plates could effectively analyze EUV light from tin LPPs across a large angular distribution (10°-90°). We ablated a planar tin target using two different laser sources and exposed two imaging plate types to ensure a thorough analysis of the IPs. IPs have the benefit of providing high-space resolution data (345 μm) compared to other techniques. High-space resolution data can be used to accurately calculate derived information such as laser energy conversion efficiency. The IP data were used to determine the laser CE to be 1.6% at Tokyo Tech. A practical and damage assessment of IPs was also given. Imaging plates are simple to use as they are light, flexible, and the size is customizable, meaning that selecting any angular distribution was possible. For high-repetition rate applications like EUVL systems that produce ions and debris, using an IP with a zirconium filter to improve IP lifetime is advisable.

ACKNOWLEDGMENTS

The authors declare that they have no competing interests. The authors would like to thank staff and researchers at ILE, Osaka, for access and assistance in experiments, particularly to Mr. Eiji Sato. The authors would like to thank the Japan Science and Technology agency for funding under the ERATO project. A part of this work was performed under the joint research project of the Institute of Laser Engineering, Osaka University.

[1]C. Wagner and N. Harned, Nat. Photonics **4**, 24–26 (2010).
[2]V. Bakshi, *EUV Source for Lithography* (SPIE, Washington, 2006), p. 4.
[3]N. M. Ceglio, A. M. Hawryluk, and G. E. Sommargren, Appl. Opt. **32**, 7050 (1993).
[4]G. E. Moore, Electronics **38**, 114 (1965).
[5]S. Owa and H. Nagasaka, Proc. SPIE **5040**, 724 (2003).
[6]W. Choi, H. Daido, S. Yamagami, K. Nagai, T. Norimatsu, and H. Takabe, J. Opt. Soc. Am. B **17**, 1616 (2000).
[7]T. Hori, Y. Kawasuji, H. Tanaka, Y. Watanabe, Y. Shiraishi, T. Abe, T. Okamoto, T. Kodama, H. Nakarai, T. Yamazaki, S. Okazaki, T. Saitou, and H. Mizoguchi, Proc. SPIE **9776**, 977625-1 (2016).
[8]A. Pirati, R. Peeters, D. Smith, S. Lok, M. van Noordenburg, R. van Es, E. Verhoeven, H. Meijer, A. Minnaert, J.-W. va der Horst, H. Meiling, J. Mallmann, C. Wagner, J. Stoeldraijer, G. Fisser, J. Finders, C. Zoldesi, U. Stamm, H. Boom, D. Brandt, D. Brown, I. Fomenkov, and M. Purvis, Proc. SPIE **9776**, 97760A-2 (2016).
[9]B. Turkot, S. L. Carson, A. Lio, T. Liang, M. Phillips, B. McCool, E. Stenehjem, T. Crimmins, G. Zhang, and S. Sivakumar, Proc. SPIE **9776**, 977602-1 (2016).
[10]P. W. Wachulak, Rev. Sci. Instrum. **87**, 091501 (2016).
[11]W. Li, L. Urbanski, and M. C. Marconi, Rev. Sci. Instrum. **86**, 121301 (2015).
[12]S. G. Gales and C. D. Bentley, Rev. Sci. Instrum. **75**, 4001 (2004).
[13]Z. Li, H. Daido, A. Fukumi, A. Sagisaka, K. Ogura, M. Nishiuchi, S. Orimo, Y. Hayashi, M. Mori, M. Kado, S. V. Bulanov, T. Zh. Esirkepov, Y. Oishi, T. Nayuki, T. Fujii, K. Nemoto, S. Nakamura, and A. Noda, Phys. Plasmas **13**, 043104 (2006).
[14]G. Dunham, E. C. Harding, G. P. Loisel, P. W. Lake, and L. B. Nielsen-Weber, Rev. Sci. Instrum. **87**, 11E301 (2016).
[15]B. Nensel, P. Thielemann, and G. Decker, J. Appl. Phys. **83**, 2276 (1998).
[16]M. Yamaura, S. Uchida, A. Sunahara, Y. Shimada, H. Nishimura, S. Fujioka, T. Okuno, K. Hashimoto, K. Nagai, T. Norimatsu, K. Nishihara, N. Miyanga, Y. Izawa, and C. Yamanaka, Appl. Phys. Lett. **86**, 181107 (2005).
[17]K. Nagai, Q. Gu, Z. Gu, T. Okuno, S. Fujioka, H. Nishimura, Y. Tao, Y. Yasuda, M. Nakai, T. Norimatsu, Y. Shimada, M. Yamaura, H. Yoshida, M. Nakatsuka, N. Miyanaga, K. Nishihara, and Y. Izawa, Appl. Phys. Lett. **88**, 094102 (2006).
[18]T. Higashiguchi, M. Hamada, and S. Kubodera, Rev. Sci. Instrum. **78**, 036106 (2007).
[19]C. M. Shetty, A. Barthur, A. Kambadakone, N. Narayanan, and R. Kv, Am. J. Roentgenol. **196**, W37 (2011).
[20]Polystyrene is transparent for 1064 nm light, and is ablated by $>10^{10}$ W/cm^2 by a 1 ns pulse. By observing the ablation trace, the laser spot size can be determined; K. Nagai, H. Yoshida, T. Norimatsu, N. Miyanaga, Y. Izawa, and T. Yamanaka, Appl. Surf. Sci. **197-198**, 808–813 (2002).
[21]S. Fujioka, H. Nishimura, K. Nishihara, M. Murakami, Y.-G. Kang, Q. Gu, K. Nagai, T. Norimatsu, N. Miyanaga, Y. Izawa, and K. Mima, Appl. Phys. Lett. **87**, 241503 (2005).
[22]S. Namba, S. Fujioka, H. Nishimura, Y. Yasuda, K. Nagai, N. Miyanaga, Y. Izawa, K. Mima, and K. Takiyama, Appl. Phys. Lett. **88**, 171503 (2006).
[23]G. O'Sullivan, B. Li, R. D'Arcy, P. Dunne, P. Hayden, D. Kilbane, T. McCormack, H. Ohashi, F. O'Reilly, P. Sheridan, E. Sokell, C. Suzuki, and T. Higashiguchi, J. Phys. B: At., Mol. Opt. Phys. **48**, 144025 (2015).
[24]T. A. Johnson, R. Soufli, E. M. Gullikson, and M. Clift, Proc. SPIE **5538**, 0277786 (2004).
[25]M. J. Haugh, J. Lee, E. Romano, and M. Schneider, Proc. SPIE **8850**, 885007-01 (2013).
[26]K. Nishihara, A. Sunahara, A. Sasaki, M. Nunami, H. Tanuma, S. Fujioka, Y. Shimada, K. Fujima, H. Furukawa, T. Kato, F. Koike, R. More, M. Murakami, T. Nishikawa, V. Zhakhovskii, K. Gamata, A. Takata, H. Ueda, H. Nishimura, Y. Izawa, N. Miyanaga, and K. Mima, Phys. Plasmas **15**, 056708 (2008).
[27]Y. Shimada, H. Nishimura, M. Nakai, K. Hashimoto, M. Yamaura, Y. Tao, K. Shigemori, T. Okuno, K. Nishihara, T. Kawamura, A. Sunahara, T. Nishikawa, A. Sasaki, K. Nagai, T. Norimatsu, S. Fujioka, S. Uchida, M. Miyanaga, Y. Izawa, and C. Yamanaka, Appl. Phys. Lett. **86**, 051501 (2005).
[28]A. Curcio, P. Andreoli, M. Cipriani, G. Claps, F. Consoli, G. Cristofari, R. De Angelis, D. Giulietti, F. Ingenito, and D. Pacella, J. Instrum. **11**, C05011 (2016).
[29]S. S. Harilal, J. Appl. Phys. **102**, 123306 (2007).
[30]S. Yuspeh, Y. Tao, R. A. Burdt, M. S. Tillack, Y. Ueno, and F. Najmabadi, Appl. Phys. Lett. **98**, 201501 (2011).
[31]H. Sakaguchi, S. Fujioka, S. Namba, H. Tanuma, H. Ohashi, S. Suda, M. Shimomura, Y. Nakai, Y. Kimura, Y. Yasuda, H. Nishimura, T. Norimatsu, A. Sunahara, K. Nishihara, N. Miyanaga, Y. Izawa, and K. Mima, Appl. Phys. Lett. **92**, 111503 (2008).

[32]G. Fiksel, F. J. Marshall, C. Mileham, and C. Stoeckl, Rev. Sci. Instrum. **83**, 086103 (2012).
[33]A. Roy, G. Arai, H. Hara, T. Higashiguchi, H. Ohashi, A. Sunahara, B. Li, P. Dunne, G. O'Sullivan, T. Miura, T. Mocek, and A. Endo, Appl. Phys. Lett. **105**, 074103 (2014).
[34]L. Yin, H. Wang, B. A. Reagan, C. Baumgarten, E. Gullikson, M. Berrill, V. N. Shlyaptsev, and J. J. Rocca, Phys. Rev. Appl. **6**, 034009 (2016).
[35]G. O'Sullivan, B. Li, P. Dunne, P. Hayden, D. Kilbane, R. Lokasani, E. Long, H. Ohashi, F. O'Reilly, J. Sheil, P. Sheridan, E. Sokell, C. Suzuki, E. White, and T. Higashiguchi, Phys. Scr. **90**, 054002 (2015).